Current Research in Neurobiology 4 (2023) 100089

Contents lists available at ScienceDirect

Current Research in Neurobiology

journal homepage: www.sciencedirect.com/journal/current-research-in-neurobiology

Dynamic structural remodeling of the human visual system prompted by bilateral retinal gene therapy

Manzar Ashtari [a,b,c,*], Philip Cook [c], Mikhail Lipin [a], Yinxi Yu [b], Gui-Shuang Ying [b], Albert Maguire [a,b], Jean Bennett [a,b], James Gee [c], Hui Zhang [d]

[a] Center for Advanced Retinal and Ocular Therapeutics (CAROT), University of Pennsylvania, Philadelphia, PA, 19104, United States
[b] Department of Ophthalmology, University of Pennsylvania, Philadelphia, PA, 19104, United States
[c] Department of Radiology, University of Pennsylvania, Philadelphia, PA, 19104, United States
[d] Centre for Medical Image Computing, University College London, London, United Kingdom

ARTICLE INFO

Keywords:
Visual system
Brain plasticity
Myeline thinning
Dendritic sprouting
Retinal gene therapy

ABSTRACT

The impact of changes in visual input on neuronal circuitry is complex and much of our knowledge on human brain plasticity of the visual systems comes from animal studies. Reinstating vision in a group of patients with low vision through retinal gene therapy creates a unique opportunity to dynamically study the underlying process responsible for brain plasticity. Historically, increases in the axonal myelination of the visual pathway has been the biomarker for brain plasticity. Here, we demonstrate that to reach the long-term effects of myelination increase, the human brain may undergo demyelination as part of a plasticity process. The maximum change in dendritic arborization of the primary visual cortex and the neurite density along the geniculostriate tracks occurred at three months (3MO) post intervention, in line with timing for the peak changes in postnatal synaptogenesis within the visual cortex reported in animal studies. The maximum change at 3MO for both the gray and white matter significantly correlated with patients' clinical responses to light stimulations called full field sensitivity threshold (FST). Our results shed a new light on the underlying process of brain plasticity by challenging the concept of increase myelination being the hallmark of brain plasticity and instead reinforcing the idea of signal speed optimization as a dynamic process for brain plasticity.

1. Introduction

Leber's congenital amaurosis (LCA) is a rare inherited early onset blindness that has been associated with mutations in at least 26 different genes (https://sph.uth.edu/retnet/sum-dis.htm). One of the more common forms of LCA is associated with the gene encoding retinal pigment epithelium-specific protein 65 kDa (RPE65) and is called LCA type 2 (LCA2)(Jin et al., 2005; Moiseyev et al., 2005). As compared with some other forms of LCA, patients with *RPE65* mutations are especially good candidates for retinal gene therapy (GT) as the retinal degenerative component of the disease occurs relatively slowly thereby providing a larger potential window for intervention. Proof of safety and efficacy of gene augmentation therapy for *RPE65* mediated retinal degeneration was carried out in several phase 1 trials and one phase 3 clinical trial. Following the success of the Phase 1 (dose escalation) and Phase 1 follow-on study (gene therapy of the contralateral eye of the Phase 1 RPE65 patients), a Phase 3 clinical trial in a new group of patients with *RPE65* mutations started in October of 2012 (see Gene Therapy Clinical Trials section) at the Children's Hospital of Philadelphia (CHOP) with a second site at University of Iowa (Maguire et al., 2008, 2009). Results of the Phase 1 and 3 trials showed improvement in patients' visual function and their navigational abilities (Ashtari et al., 2011; Bennett et al., 2012) with the improvements lasting at least 3 years post treatment (Ashtari et al., 2017; Bennett et al., 2016; Maguire et al., 2019; Russell et al., 2017; Testa et al., 2013). The visual improvements and detailed clinical results on the Phase 3 clinical trial have been reported by Russell and colleagues (Russell et al., 2017) and Maguire and collaborators (Maguire et al., 2019, 2021).

Previously, we demonstrated that in RPE65 patients, the visual cortex can show functional responsiveness to visual input through unilateral ocular gene therapy (Ashtari et al., 2011) and following

* Corresponding author. Center for Advanced Retinal and Ocular Therapeutics (CAROT), University of Pennsylvania, Philadelphia, PA, 19104, United States.
E-mail addresses: ashtari@pennmedicine.upenn.edu (M. Ashtari), cookpa@pennmedicine.upenn.edu (P. Cook), lipinm@pennmedicine.upenn.edu (M. Lipin), yinxiyu@pennmedicine.upenn.edu (Y. Yu), gsying@pennmedicine.upenn.edu (G.-S. Ying), amaguire@pennmedicine.upenn.edu (A. Maguire), jebennet@pennmedicine.upenn.edu (J. Bennett), gee@upenn.edu (J. Gee), gary.zhang@ucl.ac.uk (H. Zhang).

https://doi.org/10.1016/j.crneur.2023.100089
Received 24 October 2022; Received in revised form 3 February 2023; Accepted 1 May 2023
Available online 4 June 2023

Abbreviations:

(LCA)	Leber's congenital amaurosis
(RPE)	Retinal pigment epithelium
(GT)	Gene therapy
(CHOP)	Children's Hospital of Philadelphia
(GS)	Geniculostriate
(NODDI)	Neurite Orientation Dispersion and Density Imaging
(dMRI)	diffusion MR imaging
(NDI)	neurite density index
(ODI)	neurite orientation dispersion index
(FWF)	free water fraction
(WM)	white matter
(GM)	gray matter
(CF)	calcarine fissure
(ROI)	region of interest
(IST)	intra-subject template
(PAT)	population average template
(CSF)	cerebral spinal fluid
(ALIC)	anterior limb of the internal capsule
(FST)	Full Field Sensitivity Threshold

subretinal injection to the fellow eyes (Ashtari et al., 2017; Bennett et al., 2012), even after prolonged visual deprivation of up to 47 years. Additionally, in a group of patients who received unilateral gene therapy, we also showed that structural changes caused by lack of vision are reversible upon vision restoration (Ashtari et al., 2015). Although we have successfully demonstrated that prolonged effects of low vision on the brain's structure and function are partially reversible through retinal gene therapy, the underlying mechanism by which these processes take place remain unknown. The impact of changes in visual input on neuronal circuitry is complex but as demonstrated in a recent review article (Baroncelli and Lunghi, 2021), growing number of reports show that visual cortex has a high degree of plasticity for repair which extends into the adulthood (Castaldi et al., 2020; Lunghi et al., 2019). In addition to the capacity of the human brain plasticity, similar processes has been shown in animal studies (Mataga et al., 2004; Tropea et al., 2010); (Matsuzaki et al., 2004) (Holtmaat et al., 2006; Noguchi et al., 2005; Oray et al., 2004). Although the underlying mechanism for brain plasticity is unknown, much of the animal studies have shown that dendritic spines undergo dynamic rapid changes in response to alteration in sensory input as well as during critical period (Krieger, 2009; Lendvai et al., 2000; Majewska and Sur, 2003; Oray et al., 2004). Monocular deprivation in adult animals have also been shown rapid reduction and retraction of dendritic branches (Chen et al., 2011). The decreases in the dendritic branches of the deprived eye have been shown to accompany an increase in synapses and dendritic arborization driven by the open eye (Kirkwood and Bear, 1994). The functional and structural changes due to visual deprivation were both demonstrated to be reversible upon sight restoration of the deprived eye (Medini, 2014; Yu et al., 2011).

Having access to Phase 3 clinical trial subjects who received high dose of AAV2. hRPE65v2 (Maguire et al., 2019; Russell et al., 2017), and the advanced method of diffusion imaging called NODDI (see the Methods section). NODDI has been successfully used for detecting longitudinal changes (Palacios et al., 2020) and various aspects of the NODDI's reliability and reproducibility are demonstrated earlier (Andica et al., 2018, 2020; Chung et al., 2016; Kamagata et al., 2016; Parvathaneni et al., 2018) and in recent reviews (Kamiya et al., 2020; Kraguljac et al., 2022; Lehmann et al., 2021). We had a unique opportunity to longitudinally examine the spatial and temporal patterns of brain plasticity in response to vision reversal utilizing the well-established NODDI methodology. The studies were performed as group analyses given that most eyes received subretinal injection in the similar retinal location (Superior nasal). Our primary goal was to determine if there are parallels between cortical changes reported in animal studies with reverse eye-lid suture and human retinal gene therapy (both gaining sight) particularly with respect to the short-term process of plasticity of the local dendritic architecture within the primary visual cortex (V1) and a long-term alteration of the white matter microstructure along the geniculostriate (GS) fibers connecting the lateral geniculate nucleus to V1.

1.1. Previous and current neuroimaging studies of the RPE65 clinical trials

The neuroimaging study of the Phase 3 clinical trial patients differed in several aspects from our previous reports. As compared to Phase 1, where patients received unilateral subretinal injections, patients in Phase 3 received bilateral subretinal injections, 6–18 days apart (Maguire et al., 2021; Russell et al., 2017). The average age for Phase3 neuroimaging participants was 14 years and for Phase 1 and Phase 1/2 was 22 years. In Phase 3, we were able to capture subjects' baseline scan, which was not available in the other two studies. In Phase 3, patients were followed up at four different time points (1, 3, 6, and 12 months after intervention) allowing a unique opportunity to evaluate the temporo-structural impact of changes in visual input on neuronal circuitry and assess both the early and long-term microstructural alterations of the visual pathway in response to vision restoration.

Based on the rapid and long-term phases of structural plasticity identified in animal studies, we hypothesize that the process of brain plasticity in the RPE65 patients, prompted by vision restoration through retinal gene therapy, starts by remodeling of the dendritic trees within the V1 followed by experience-dependent synaptic plasticity within the white matter microstructure of the visual pathway. To assess this two-step process of brain plasticity, RPE65 patients were evaluated in a longitudinal neuroimaging study employing an advanced method of diffusion imaging called Neurite Orientation Dispersion and Density Imaging (NODDI)(Zhang et al., 2012). Through NODDI parameters we assessed microstructural changes of the dendritic tree in V1 and using tractography evaluated the effect of vision restoration on the GS fibers connecting the lateral geniculate nucleus to the visual cortex.

2. Materials and methods

2.1. Gene Therapy Clinical Trials

A controlled randomized Phase 3 clinical trial incorporating sequential bilateral subretinal administration of the recombinant adeno-associated virus (AAV) carrying the wildtype *RPE65* cDNA was jointly launched at the Children's Hospital of Philadelphia (CHOP) and the University of Iowa (UI). Patients greater than 3 years old with a confirmed genetic diagnosis of bi-allelic *RPE65* mutations and a visual acuity of 20/60 or worse in both eyes were recruited in the Phase 3 clinical trial. A total of 31 patients between the ages of 4–44 years were recruited in the study of which 29 were treated and followed over time (Russell et al., 2017). Subretinal injection was performed first in the worse seeing eye followed by the injection of the second eye, 6–18 days later (Russell et al., 2017). All patients received the same dose of $1.5x10^{11}$ vg in a total subretinal injection volume of 0.3 mL in each eye (Russell et al., 2017). The voretigene neparvovec-rzyl was delivered to the superior nasal aspect of retina about two disk diameters (optic disk) from the fovea in nearly all subjects. Results from the phase 3 clinical trial showed improvement in patients' light sensitivity, visual fields and navigational ability under dim light (Russell et al., 2017).

2.2. Study participants

Ten/26 of the RPE65 patients, older than 7 years, elected to participate in the neuroimaging study. One patient who was diagnosed with

ADHD and had excessive motion on particularly the diffusion images was later removed from the study group. Additionally, eight demographically matched controls were recruited. All matched control volunteers were recruited through IRB-approved advertisements. Exclusion criteria for controls consisted of current or past psychiatric diagnosis, history of alcohol or drug abuse, known neurological disorders, history of head injury, or current use of psychotropic medications. All subjects provided written informed consent (>18Yrs) or written assent and parental permission (<18Yrs). This study was Health Insurance Portability and Accountability Act of 1996 compliant and approved by the IRB at CHOP and UPenn. RPE65 patients and controls did not significantly differ in age, gender, and handedness (Table 1). All RPE65 patients were enrolled from the CHOP-site. A more detailed patients' demographic and information regarding subretinal injections are presented in Table S1of the Supplementary Information.

2.3. Neuroimaging protocol

MRI scans were conducted at CHOP on a 3 T S Verio system equipped with a 32-channel head coil. Subjects' head were secured using foam padding to reduce head motion and scans were monitored to be artifacts free at acquisition time. All subjects underwent a magnetization prepared rapid acquisition gradient echo (MPRAGE) 3D and a group of advanced diffusion MR imaging (dMRI) sequences. Patients received MRI at baseline, 1-, 3-, 6- and 12-months post-intervention and controls underwent MRI at baseline and 1 year.

2.3.1. 3D-MPRAGE

Sequence parameters included repetition time (TR) = 2080ms, echo time (TE) = 2.54ms, bandwidth = 180 Hz/Px, matrix size = 320x320, field of view = 256 × 256mm^2, number of slices = 192, slice thickness = 0.8 mm, inversion time = 1200ms with Flip Angle = 8°, number of excitations = 1, integrated Parallel Acquisition Techniques (iPAT) factor = 2 and total acquisition time = 7:04 min.

2.3.2. Diffusion-MRI

dMRIs were acquired with a multi-shell spherical sampling scheme with 2x2x2 mm^3 isotropic voxels. The two shells were 18 directions with low b-values (700 s/mm^2 or 1000 s/mm^2), followed by 32 or 36 directions with high b-values (2000 s/mm^2), and 3 additional b0-images. To maintain constant signal to noise, TE = 90ms was maintained across all diffusion series.

Table 1
Demographic characteristics in RPE65 patients and controls.

	Patients (N = 9)	Controls (N = 8)	p value
Age at Baseline (Year)			0.89[a]
N	9	8	
Mean (SD)	13.8 (5.7)	13.4 (6.0)	
Median	13.0	11.0	
Q1, Q3	10.0, 18.0	9.0, 18.0	
Range	(7.0–24.0)	(8.0–23.0)	
Gender			0.62[b]
Female	5 (55.6%)	6 (75.0%)	
Male	4 (44.4%)	2 (25.0%)	
Race			0.21[b]
Caucasian	9 (100.0%)	6 (75.0%)	
Non-Cauca	0 (0.0%)	2 (25.0%)	
Handedness			1.00[b]
Ambidexter	1 (11.1%)	1 (12.5%)	
Left	1 (11.1%)	0 (0.0%)	
Right	7 (77.8%)	7 (87.5%)	

[a] *t*-Test.
[b] Fisher Exact Test.

2.3.3. Neurite Orientation Dispersion and Density Imaging (NODDI)

NODDI is an advanced dMRI analysis technique for imaging tissue microstructure in both gray and white matter (Zhang et al., 2012). It is the first technique that can directly estimate neurite density index (NDI), neurite orientation dispersion index (ODI), and free water fraction (FWF), suitable for clinical imaging. Unlike the standard dMRI parameters, NODDI presents specific information related to changes of tissue microstructure and it provides direct measures for the density and direction of axons within white matter (WM) and provide information on dendrite dispersion within gray matter (GM). For example, in WM neurite density is high and orientation dispersion is low, in areas containing bundles of mostly co-linear axonal fibers. In cortical gray matter, neurite density is lower, but orientation dispersion is much higher, because the neurite orientations do not cluster tightly around a single axis as they do in the major white matter tracts. It is important to note that NODDI metrics such as ODI and NDI have been shown to provide more biologically specific sensitivity as compared to the traditional diffusion parameters of the fractional anisotropy (FA), axial (AD), radial (RD) and mean diffusivity (MD) (Chang et al., 2015; Timmers et al., 2016; Young et al., 2019). Comparison of the NODDI parameters with traditional diffusion metrics (e.g. FA, MD, RD) in the current study (not included in the results) showed similar high sensitivity for NODDI as compared to DTI parameters. In fact, in the absence of using NODDI, results presented in the current study would not have been possible. The reliability and reproducibility of the NODDI method, in particular the ODI and NDI parameters, are reported in recent review articles (Kamiya et al., 2020; Kraguljac et al., 2022). In addition, NODDI has been employed in a range of imaging studies, such as normal ageing (Nazeri et al., 2015), neurodegenerative diseases (Andica et al., 2018; Colgan et al., 2016; Kamagata et al., 2016), stroke (Adluru et al., 2014), cortical dysplasia (Winston et al., 2014), first-episode psychosis (Rae et al., 2017), and recently presymptomatic phase of C9orf72 disease (Wen et al., 2019).

2.3.4. Gray matter template construction and ROI extraction

Visual impairment has considerable impact on the brain's visual pathways, mainly resulting in abnormality within the V1 areas. As such, GM located around the calcarine fissure (CF) (Purves et al., 2001), was selected as the region of interest (ROI) to examine the effects of retinal gene therapy on V1 dendritic arborization. To extract the ROIs an unbiased intra-subject template (IST) was constructed from the T1-images of each subject at multiple time points using ANTs software (Tustison and Avants, 2013). Individual ISTs were then combined to build a T1 population average template (PAT), with the aim of creating one ROI for both controls and patients. However, due to the presence of retinal disease the exact location of the CF in the PAT space dramatically varied among patients as compared to controls. But using the individual IST templates, the CF was clearly resolved for all subjects, indicating the accuracy of longitudinal alignment for multiple time points. To exclude voxels contaminated by the cerebral spinal fluid (CSF), the ISTs were registered to the NODDI-FWF IST template which accurately depicts CSF spaces. The ROIs were then superimposed onto the FWF template and manually edited to exclude any voxel containing CSF. Fig. 1 shows the selected GM-ROIs in the V1 areas for three slices within the left and right hemispheres for the superior (blue) and inferior (yellow) pericalcarine tissues superimposed onto the NODDI-FWF template. The CSF borders defining the CF is shown in green. For comparison, a non-visual area, motor cortex GM was extracted in both the left and right hemispheres using the same approach used to extract the V1-ROIs. More details regarding the T1-NODDI registration along with the schematic diagram (Fig. S1) showing the steps of registration are presented in the SI. The exact details for the extraction of the motor GM ROIs are presented in the SI.

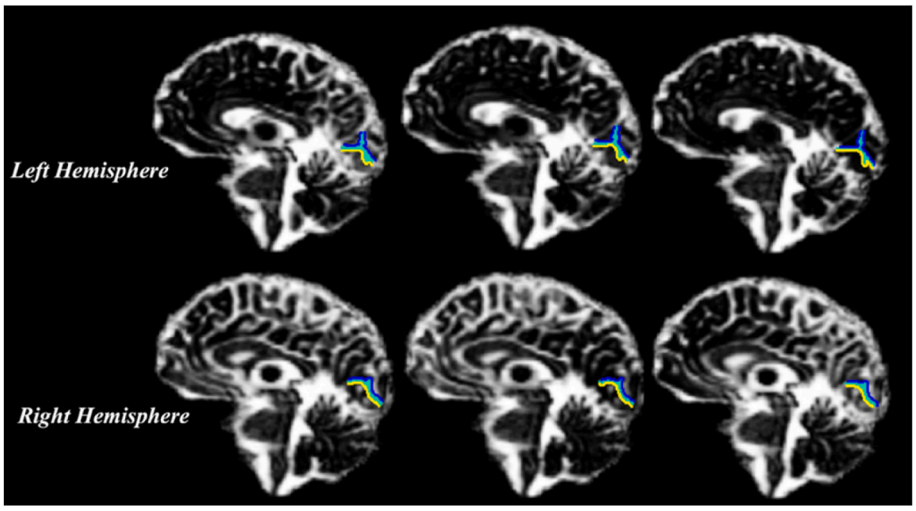

Fig. 1. Delineation of the superior (blue) and inferior (yellow) pericalcarine gray matter tissue as the primary visual cortex (V1) regions of interest superimposed onto the NODDI free water fraction (FWF) template. (For interpretation of the references to color in this figure legend, the reader is referred to the Web version of this article.)

2.3.5. White matter template construction and ROI extraction

The major fiber bundles relaying the visual information to V1 areas are GS tracts. Unlike the calcarine ROIs, the GS tracts are easily identified in single subjects and do not have drastic location variance among subjects. As such, the diffusion PAT images (template from all subjects) were used to perform tractography and isolate the GS tracts as the WM-ROIs. The PAT WM template was constructed using the dMRIs. Diffusion Images were first distortion and motion corrected using FSL Diffusion Toolbox (Andersson and Sotiropoulos, 2016) and raw diffusion images. The NODDI model was then fit to the corrected data (see SI section) to create the tensor images which was used to construct a WM template using DTI-TK Toolbox (Zhang et al., 2006). The NODDI-Toolbox (Zhang et al., 2012) was then used to generate the NDI, ODI and FWF scalar images. The details of parameter derivation for the NODDI model are described elsewhere (Zhang et al., 2012) and the flowchart for WM template creation (see Fig. S2) is presented in the SI. Using the PAT images and the DSI Studio (Yeh et al., 2013) GS tracks were reconstructed via deterministic streamline tractography. A combination of inclusion and exclusion planes were used to extract the GS tracts and shown in Fig. 2. The detailed parameters used for tract extraction are presented in the SI section.

As with the experiments in gray matter, we used a bilateral control regions for WM, specifically the left and right anterior limb of the internal capsule (ALIC), from a standard white matter atlas (Mori et al., 2005). The extracted control WM-ROIs are presented in Fig. S4, and the detailed of extraction for these control tracts is presented in the SI.

3. Statistical analysis

Based on a one-to-one relation between the superior and inferior retina and the superior and inferior pericalcarine tissue and the hemispheric trajectories of the nasal and temporal retinal fibers, the superior and inferior pericalcarine tissue for each hemisphere and the left and right GS fibers were analyzed separately. All statistical analyses were performed using SAS version 9.4 (SAS Institute Inc., Cary, NC). Microstructural changes of the gray and white matter over time were assessed separately for the left and right hemispheres ROIs using the longitudinal regression analysis through linear mixed effects (LME) models. In LME models, autoregressive (AR1) correlation structure was used to adjust for the correlation among longitudinal repeated measures (Laird and Ware, 1982) for the RPE65 patients and matched controls separately. Time points included in the longitudinal analysis for patients were baseline, 1-, 3-, 6-, and 12-months post intervention and for controls were baseline and 12 months. Time was modelled as categorical variable to avoid any assumption on the linear change over time for these measures. From linear mixed effects models for data from the RPE65 patients, the p-values for any difference (e.g., overall p-value) across all five time points (baseline, 1-, 3-, 6-, and 12-months) were calculated. When the overall longitudinal statistical comparisons were statistically significant (e.g., overall $p < 0.05$), the post-hoc comparison of baseline vs. each post intervention time point (1, 3, 6, and 12 months) were made. The Hochberg (1988) procedure (a less conservative, more powerful procedure than the Bonferroni method) was used to adjust the P values (p_c) from multiple comparisons (e.g., total of 4 comparisons for

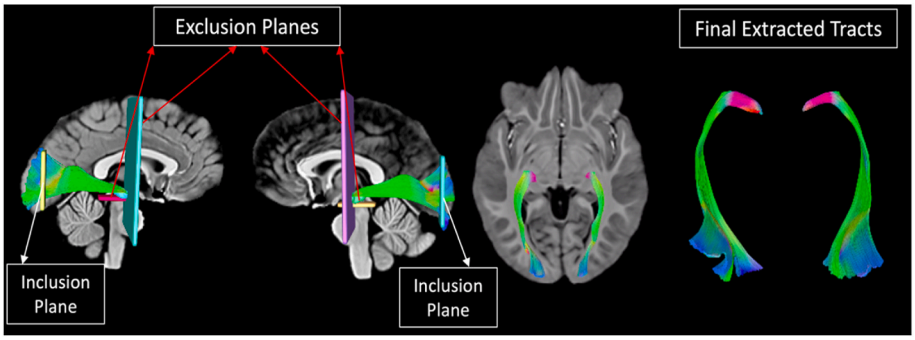

Fig. 2. Locations of the inclusion (occipital planes) and exclusion (anterior to the left and right lateral geniculate nucleus and superior to the left and right pons) ROIs and the final extracted GS tracts for the left and right hemispheres.

each outcome) and to control the overall type I error of 0.05 (2-sided). For the longitudinal analysis of data from matched controls, no post-hoc comparisons were made because there were only two time points (baseline and 12 months). All these longitudinal analyses were performed through Proc Mixed in SAS v9.4 (SAS Institute Inc, Cary, NC), and the post-hoc pairwise comparisons were performed through Estimate statement in Proc Mixed. The calculation of adjusted p-value (p_c) through Hochberg procedure was performed through Proc Multtest in SAS.

Pearson correlation analyses were performed for evaluating cross-sectional correlation between ODI, NDI and the clinical measures for the patients' Full Field Sensitivity Threshold (FST) (Roman et al., 2005) responses to the red, blue, and white colors, separately for each eye and time points. Because the nature of these correlation analyses is exploratory, we report the correlation results that are not corrected for the multiple comparisons, as well as the corrected p-values from multiple correlation analyses for each eye and color through Hochberg procedure using Proc Multtest in SAS v9.4. Because this project is the ancillary study of the clinical trial, no sample size/power calculation were performed before the start of this study. However, the post-hoc calculation indicated that the study of 9 patients provides 80% power to detect effect size of 1.1 for the longitudinal change of gray matter.

4. Results

4.1. Longitudinal gray matter analyses

As depicted in Table 2, results showed significant changes over time for the total (left + right) inferior pericalcarine ($p = 0.009$) ROI, but no significant changes were observed for the total superior pericalcarine ($p = 0.44$). Analyzing each hemisphere separately, the right inferior pericalcarine had an overall significant ($p = 0.008$) increase in ODI value with the left at trend level ($p = 0.10$).

Since the overall longitudinal measures for the total ODI of the inferior pericalcarine tissue was significant ($p = 0.009$), the individual patient's trajectory of GM changes over time for the total ODI values of the inferior pericalcarine tissue were plotted against time. As shown in Fig. 3A, most patients presented with an ODI increase for the total inferior pericalcarine GM at 3MO but not the superior portion. The averaged ODI for the total inferior pericalcarine tissue were also plotted and is presented in Fig. 3B and showed the greatest change at 3MO.The mean (standard error) of the total (right + left) inferior calcarine tissue ODI change at 3MO as compared to the baseline ODI value was 0.025 (0.099). A post-hoc analyses of the ODI measures as compared to the baseline values were performed for all time points (see Table S2) and results showed significant change only for the 3MO time point (see Table S2). Comparison was performed for both uncorrected (p) and corrected (p_c) for multiple comparisons. As depicted in Table S2, comparison of the total inferior ODI values at 3MO to the baseline values showed a significant increase in dendritic orientation dispersion ($p = 0.01$, $p_c = 0.04$; see Table S2) post retinal intervention. The ODI values of the total superior pericalcarine tissue for individual patients and averaged for all patients are presented in Fig. 3C and D respectively and show a similar peak at 3MO but the ad-hoc analyses showed no statistical significance. The longitudinal analyses of the superior and inferior calcarine tissues for control subjects did not present with any statistically significant changes over time (see Table 2).

4.2. Full field sensitivity threshold (FST)

The full Field Sensitivity Threshold (FST) is one of the clinical tests for the RPE65 patients that was designed in planning for the LCA clinical trials (Roman et al., 2005) and has been used as an outcome measure to assess the efficacy of the clinical trials (Bennett et al., 2012, 2016; Jacobson et al., 2012; Maguire et al., 2021; Russell et al., 2017). FST measures sensitivity of the entire visual field (full field stimulus) by recording patient's response to the lowest luminance of a flash with red, blue, and white colors separately. The two colors of red and blue are used to estimate the level of rods and cones dysfunctions and the white color is used for mixed photoreceptors (Roman et al., 2005; Roman et al., 2022). Using the FST responses and a sophisticated algorithm it can be determined if patients have remnant rod or cone visions and which photoreceptors are affected most (Roman et al., 2005). The FST tests were administered three times for each color at baseline, 1-, 3-, 6-, and 12-months post intervention for the left and right eye separately. The subjects were asked to indicate, by pressing a button, when they were able to perceive the stimulus. The individual responses for the FST tests for all three stimuli from the left and right eye are presented in Fig. 4. As depicted in Fig. 4, FST responses significantly improved post intervention for all three colors ($p = 0.001$) particularly for the blue and white (see Table S3) as compared to red color. This is expected as RPE65 gene predominantly affects rod photoreceptors (which are more sensitive to blue and white colors). Cones are not as dependent on RPE65 gene and thus there's not as much change with the red stimuli (Roman et al., 2005). Interestingly, Fig. 4 also shows a non-significant trend of increased FST response to blue and white stimuli at 3MO.

Table 2
Longitudinal evaluations of the pericalcarine gray matter from baseline, 1MO, 3MO, 6MO and 1 YR post bilateral administration for retinal gene therapy of a group of RPE65 patients and a group of matched controls tested at baseline and one year. Results show significant overall microstructural changes in the V1 areas of the right inferior ($p = 0.008$) and total inferior pericalcarine GM tissue ($p = 0.009$). No significant changes were observed for the GM changes over time for the superior aspect of the pericalcarine tissue. Longitudinal evaluations of pericalcarine tissue in control group also did not present with significant changes of gray matter in this area.

Orientation Dispersion Index (ODI)	Left Inferior Pericalcarine		Left Superior Pericalcarine		Right Inferior Pericalcarine		Right Superior Pericalcarine		Total Inferior Pericalcarine		Total Superior Pericalcarine	
Participants	Patient	Controls	Patient	Controls	Patient	Controls	Patient	Controls	Patient	Controls	Patient	Controls
Time	*Mean (SD)*		*Mean (SD)*		*Mean (SD)*		*Mean (SD)*		*Mean (SD)*		*Mean (SD)*	
Baseline	0.55 (0.04)	0.56 (0.03)	0.53 (0.05)	(0.05) (0.03)	0.56 (0.02)	0.54 (0.04)	0.56 (0.04)	0.54 (0.07)	0.55 (0.02)	0.55 (0.04)	0.55 (0.04)	0.55 (0.05)
1MO	0.55 (0.03)		0.55 (0.04)		0.56 (0.03)		0.57 (0.03)		0.55 (0.02)		0.56 (0.03)	
3MO	0.55 (0.03)		0.56 (0.04)		0.58 (0.03)		0.56 (0.04)		0.58 (0.03)		0.56 (0.04)	
6MO	0.55 (0.03)		0.55 (0.05)		0.56 (0.03)		0.54 (0.06)		0.56 (0.02)		0.55 (0.05)	
1 YR	0.56 (0.05)	0.56 (0.06)	0.55 (0.04)	0.54 (0.04)	0.56 (0.03)	0.53 (0.04)	0.56 (0.04)	0.52 (0.06)	0.56 (0.03)	0.55 (0.05)	0.55 (0.04)	0.53 (0.05)
P-Value	0.10	0.89	0.44	0.36	**0.008**	0.75	0.41	0.78	**0.009**	0.73	0.44	0.42

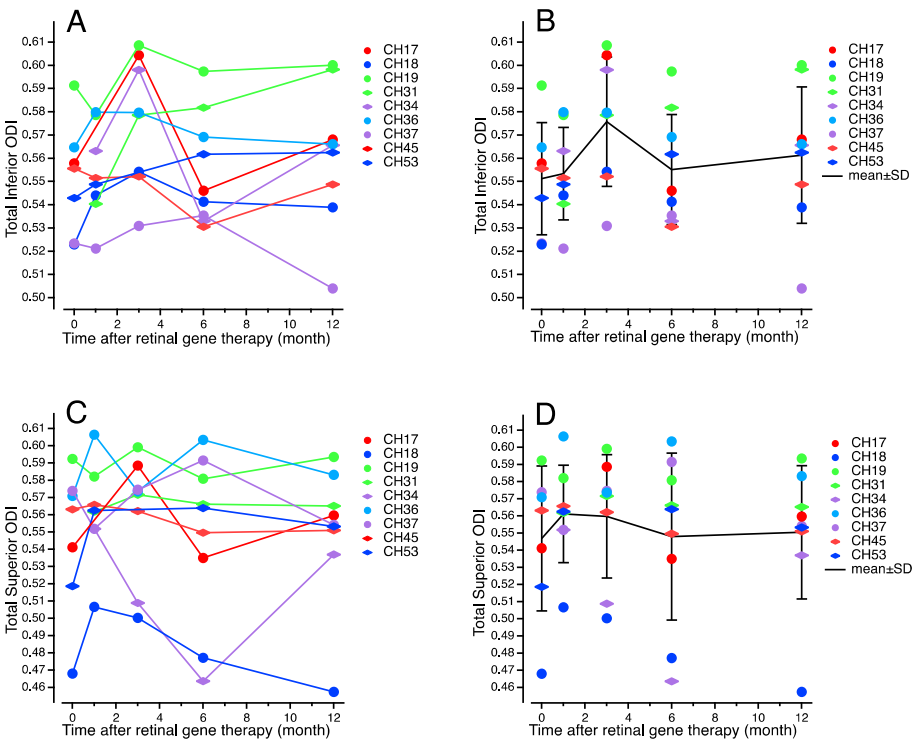

Fig. 3. Analyses of the total inferior and superior dendritic dispersion of V1 over time. **A:** Changes in the total inferior gray matter of the pericalcarine tissue for individual RPE65 patients. **B:** The overall changes in the gray matter microstructure of the total inferior pericalcarine tissue was significant ($p = 0.009$) across time with a significant peak at 3MO post intervention ($p = 0.01$; $p_c = 0.04$). **C:** The microstructural changes in the gray matter of the total superior pericalcarine tissue for individual patients. **D:** Longitudinal regression analyses of the microstructural gray matter in the superior calcarine tissue showed no significant changes over time.

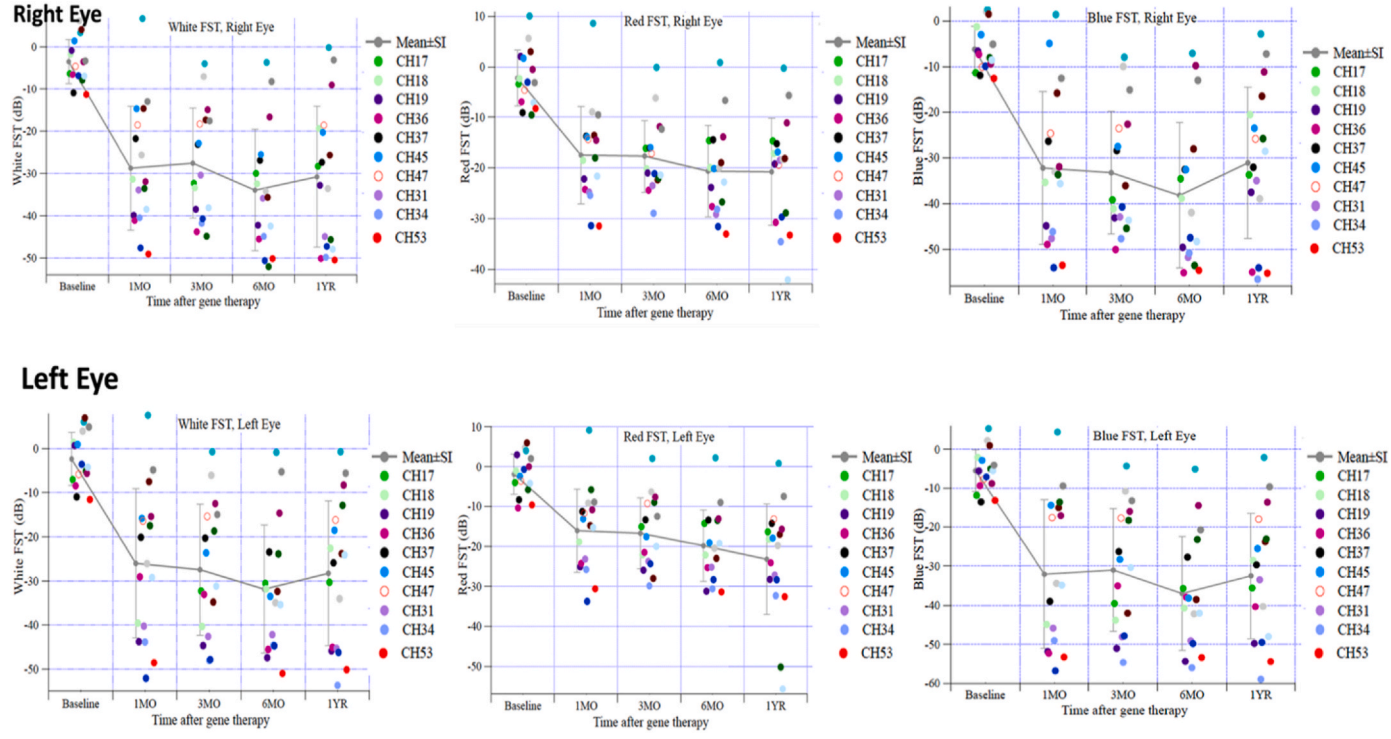

Fig. 4. The FST responses to the red, white, and blue color stimuli for the right (Top Row) and left (Bottom Row) eyes. The RPE65 patients' FST responses for red, white, and blue colors at baseline and 1-, 3-, 6- and 12-months post-intervention. As compared to the baseline, RPE65 patients showed a dramatic increase in response to all three colors after retinal gene therapy. Overall, RPE65 patients showed higher sensitivity to the blue and white light stimulations as compared to the red color. Interestingly, as compared to baseline, there appear to be a peak in the FST responses to blue and white colors at 3MO from both eyes. However, the changes were not statistically significant perhaps due to large variation in FST responses. (For interpretation of the references to color in this figure legend, the reader is referred to the Web version of this article.)

4.3. Correlations between gray matter and patients' FST responses

The Pearson correlation was used to evaluate the association between the ODI values of the total superior and inferior pericalcarine gray matter with the left and right eye clinical FST responses to the red, white, and blue color stimuli and results are presented in Fig. 5. The correlation coefficient and p-value for 3MO post intervention results are shown at the bottom of the graphs for each eye and each color separately. Correlation coefficients, the p-values uncorrected and corrected for multiple comparisons using the Hochberg method for all time points between the inferior and superior calcarine tissues and the patients' FST responses are presented in Tables S4 and S5 respectively. As shown in Fig. 5, there were significant correlations between the total inferior pericalcarine tissue ODI and both the white and blue color stimuli, for both the left and the right eye, at 3MO, whereas the correlations for the red stimulus were borderline or not significant. As presented in Table S4, correlation coefficients between the.

ODI values and the FST measures were all not statistically significant after correcting for multiple correlation analyses. However, the corrected p-value (p_c) for 3MO time point was much lower than p_c values for other time points (see Table S4). No significant correlations were observed between the total superior pericalcarine tissue ODI and the patients' left and right eye FST results for all time points (see Table S5).

4.4. Longitudinal white matter analyses

Like the GM analyses, the linear mixed effects models were used to assess the WM microstructural changes along the GS tracts over time for the RPE65 patients and controls. As depicted in Table 3, RPE65 patients showed significant ($p = 0.03$) WM changes over time for the right GS tract but not the left. Since the overall statistical comparison for the NDI measures of the right GS tract was significant, the measure was plotted against time and the largest NDI changes were observed at 3MO time point (Fig. 6). A post-hoc analysis showed a largest decrease for the NDI values of the right GS tract to be significant ($p = 0.04$) at the 3MO time point post retinal treatment. The estimated mean (standard error) change for the magnitude of the NDI values of the right GS tract from

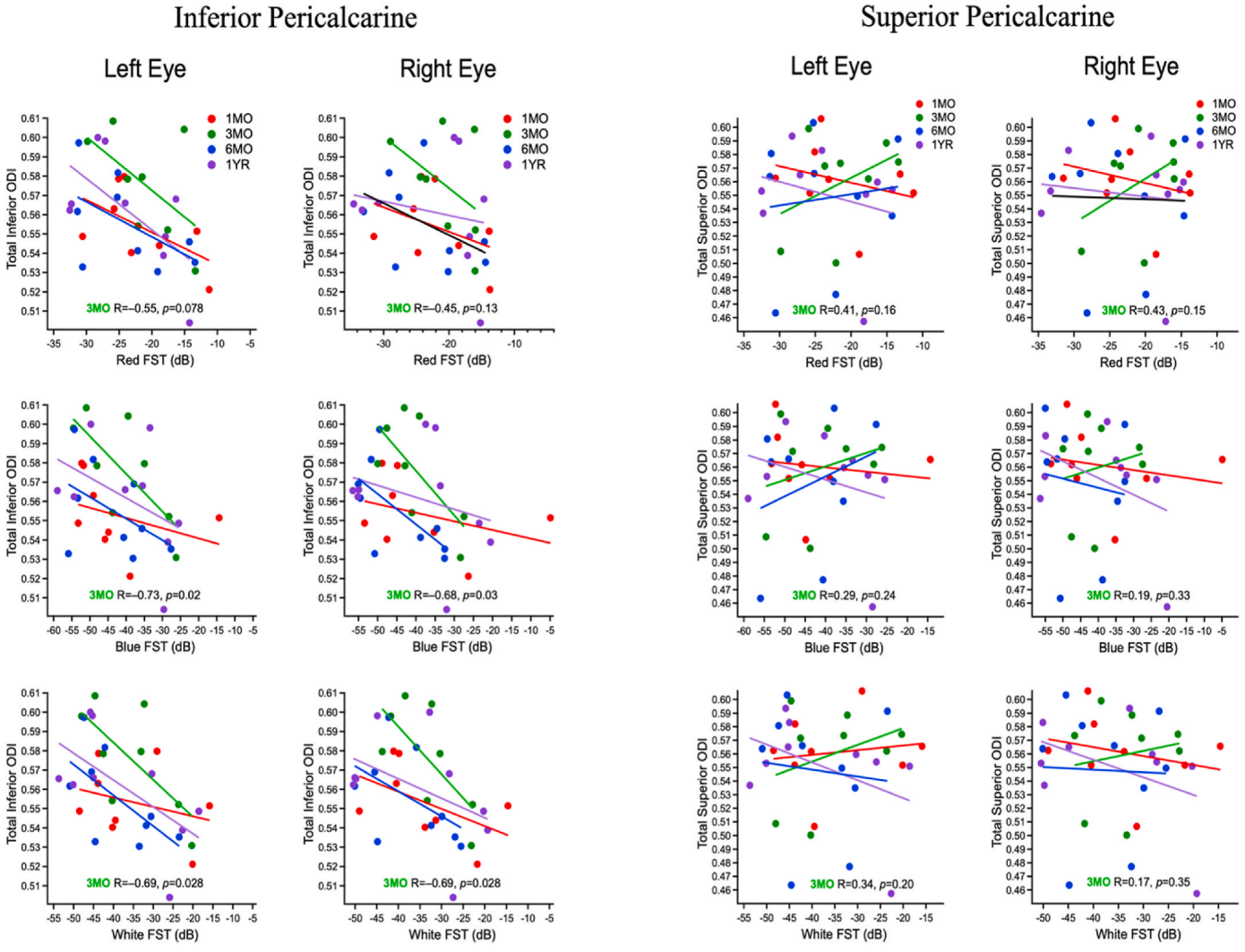

Fig. 5. Correlations of the total ODI values of the inferior and superior pericalcarine gray matter tissue for the left and right hemispheres with the patients' FST clinical measure for three colors of red, white, and blue. Results showed significant negative correlations, at 3MO time point, between the total inferior pericalcarine tissue and FST measures (Left panel) for the blue and white colors and for both the left and right eyes. Correlation coefficients for the red color FST measures did not reach significance. As presented on the right panel, no significant correlations at 3MO were observed between the total superior pericalcarine tissue and any FST measures for either the left or right eye (see Table S5). The correlations between the inferior and superior pericalcarine ODI values and patients' FST measures uncorrected and corrected for multiple comparisons for all other time points are presented in Tables S4 and S5 respectively in the Supplementary Information. (For interpretation of the references to color in this figure legend, the reader is referred to the Web version of this article.)

Table 3
Longitudinal evaluations of white matter microstructural changes along the GS tracts over time for patients and controls. Results show significant overall changes of the right geniculostriate tract ($p = 0.03$) in patients. No significant changes were observed for the left tract ($p = 0.13$). The linear mixed effect model for the post-hoc comparison showed most significant white matter microstructural changes to occur at 3MO post intervention along the right tract ($p = 0.04$). Though, the NDI comparison of the right GS tract between 3MO and baseline became non-statistically significant after correcting for multiple comparisons ($p_c = 0.16$; see Table S6). White matter microstructural changes for control group showed increase in the mean neurite density for both the left and right tracts over time, with the left tract reaching significant ($p = 0.02$). Increase in the neurite density along the geniculostriate tracts in controls maybe attributed to the process of normal development, particularly that average age for the control group around 13 years (see Table 1).

Neurite Density Index (NDI)	Left Geniculostriate Tract		Right Geniculostriate Tract	
Participants	Patients	Controls	Patients	Controls
Time	*Mean (SD)*		*Mean (SD)*	
Baseline	0.56 (0.03)	0.57 (0.05)	0.56 (0.03)	0.55 (0.04)
1MO	0.54 (0.02)		0.54 (0.02)	
3MO	0.53 (0.03)		0.52 (0.02)	
6MO	0.55 (0.04)		0.55 (0.04)	
1 YR	0.57 (0.03)	0.60 (0.04)	0.57 (0.03)	0.58 (0.04)
P-Value	0.13	**0.02**	**0.03**	0.14

baseline to 3MO post treatment was −0.03 (0.014). The traditional diffusion index of fractional anisotropy (FA) was also analyzed, and it showed no significant changes for WM along either the right or left GS tracts over time.

Results of the mixed effects modelling for the WM changes of the left and right GS tracts among controls is also shown in Table 3. As compared to baseline, the NDI values for both the left and right GS tracts in controls increased at 1 YR follow up, with the left GS tract changes over time reaching statistical significance ($p = 0.02$).

To observe the trajectory of change for individual patients, the microstructural the NDI values of the left and right GS tracts for individual patients were plotted against time and results are presented in Fig. 6A&C respectively. Most patients showed lower NDI value for the left and right GS tract at 3MO post intervention. However, as shown in Fig. 6B&D the mean microstructural changes along the right tract was more significant at 3MO ($p = 0.04$).

4.5. Correlations between white matter and patients' FST responses

The Pearson correlations was used to evaluate the association between the WM changes along the GS tracts with both the right and left eye clinical FST test results are presented in Fig. 7. The correlation coefficients along with uncorrected (p) and corrected (pc) p-value for multiple comparisons using the Hochberg method (Hochberg, 1988) for the right and left GS tracts are presented in Tables S7 and S8 of the Supplementary Information respectively. Correlation results for the NDI values at 3MO with the patients' FST responses for all three colors are indicated at the bottom for the right GS and at the top portion for the left GS tract in Fig. 7. As depicted in Fig. 7 significant positive correlations were observed for the right GS-NDI values and the blue FST responses for the left ($p = 0.047$) and right ($p = 0.05$) eyes at 3MO. The 3MO correlation between the right GS-NDI values and the white FST responses were also significant for the left eye ($p = 0.025$) and at trend level for the right eye ($p = 0.08$). As shown on the right panel of Fig. 7, the correlations for the left GS-NDI values and the FST response was significant only for the white color stimuli of the left eye ($p = 0.047$). However, after correcting for multiple comparisons, none of the correlations reached statistical significance. Although, the p-values for multiple comparisons corrections (p_c) at 3MO were smaller as compared to

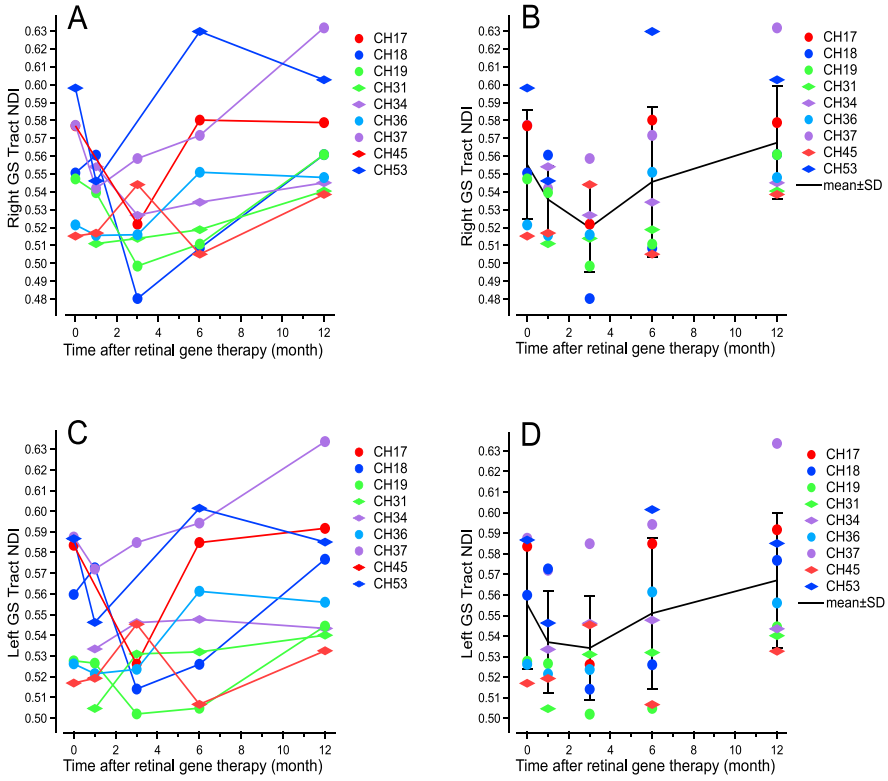

Fig. 6. Changes of the left and right GS tracts' NDI values over time in RPE65 patients. **A)** The right GS tract NDI values from baseline to 1-year post intervention for individual RPE65 patients. **B)** The mean values for the right GS tract NDI values at various time points before and after retinal intervention. **C)** The left GS tract NDI values from baseline to 1-year post intervention for individual RPE65. **D)** The mean values for the left GS tract NDI values at various time points before and after intervention. While both the right and left GS tracts showed similar trajectories over time with a dip at 3MO, only the changes in the right GS tract reached overall statistical significance ($p = 0.03$) and post hoc analysis showed largest change occur at 3MO ($p = 0.04$, $p_c = 0.16$ see Table S6) as compared to the baseline NDI values. No significant changes were observed for the NDI values of the left GS tract.

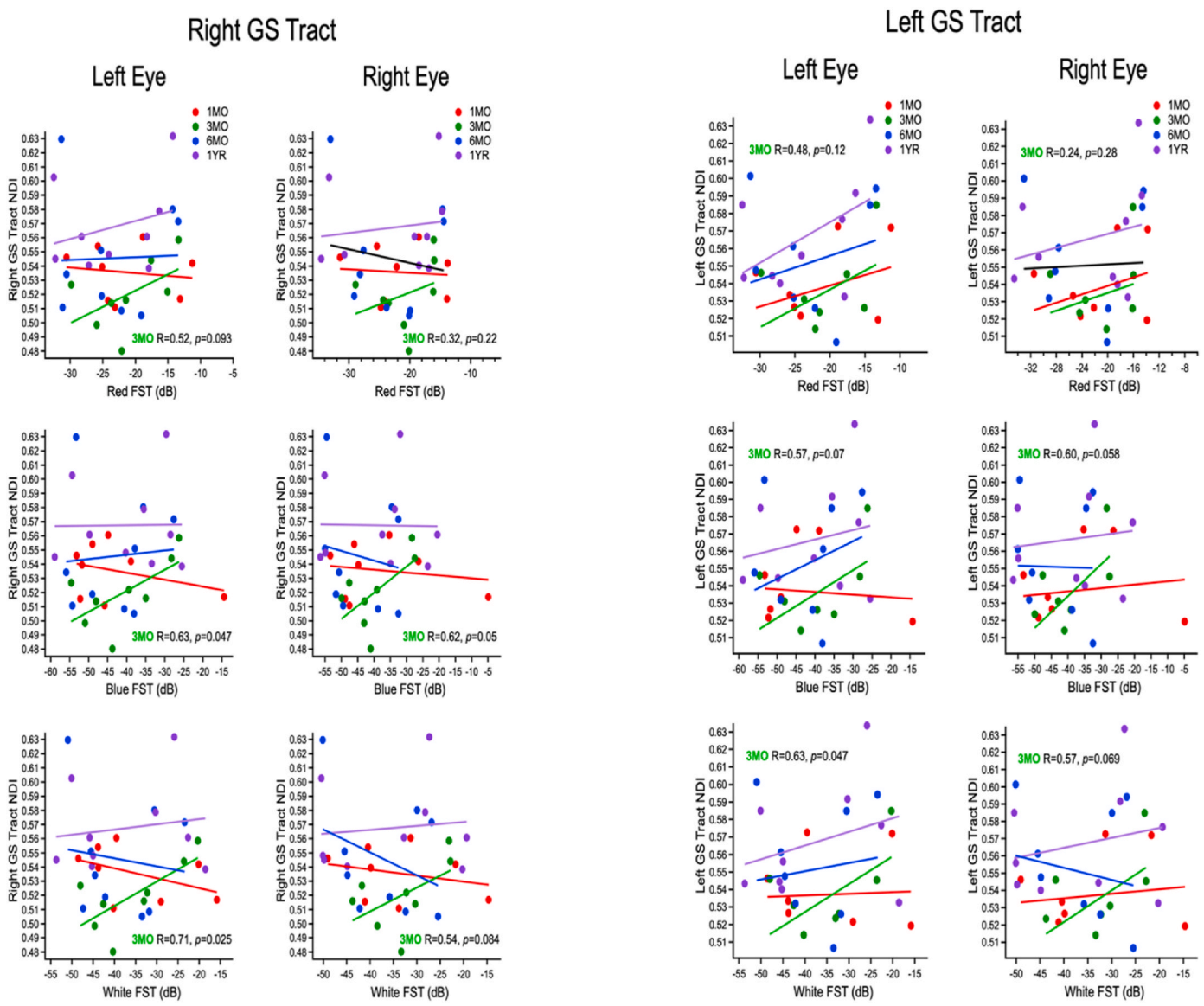

Fig. 7. Pearson correlations between patients' FST responses and neurite density along the geniculostriate tracts. Correlation coefficients along with uncorrected (p) and corrected (p_c) for multiple comparisons for all time points are presented in Table S7&S8, only the 3MO time point correlations are depicted on figures. As shown here, significant positive correlations were observed mainly for the right GS tract and the left eye FST responses to white (p = 0.025) and blue (p = 0.047) stimuli. These correlations did not survive the correction for Hochberg multiple comparisons. Note that positive correlation here means negative association between the NDI and FST. Thus, higher neurite density correlated with poor FST responses, particularly at 3MO, whereas the baseline correlations (not shown, see Table S7) were significantly negatively correlated with almost all FST responses, demonstrating an opposite relationship to what is observed at 3MO. Observation at baseline is the expected association where the higher neurite density correlates with higher FST sensitivity. (For interpretation of the references to color in this figure legend, the reader is referred to the Web version of this article.)

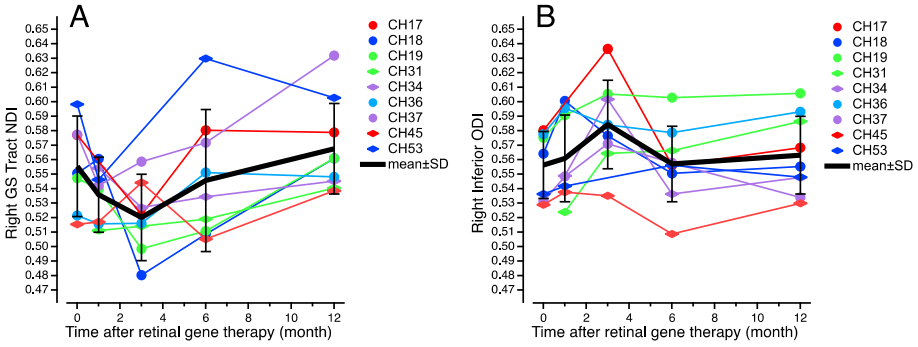

Fig. 8. The single subject longitudinal changes of the right GS-NDI and the right inferior pericalcarine ODI values. Although, these individual changes in GM and WM were previously shown in Figs. 3A and 6A, for a better side by side comparison they are presented in as a separate figure as well. This side-by-side comparison show that both NDI (Panel A) and ODI (Panel B) values for individual RPE65 patients changed in opposite directions and transitioned through a significant change at exactly 3MO time point for ODI of the right pericalcarine tissue (p = 0.02) and the NDI of the right GS tract (p = 0.04).

the corrected p-values for other time points. As shown in Fig. 7, correlations for the NDI values of both the left and right GS tracts and the responses to the red stimuli were mostly not significant.

4.6. 3MO time point post retinal intervention changes of the gray and white matter

Fig. 8, (a combination of Figs. 3A and 6A) shows a side-by-side comparison of the WM and GM microstructural changes over time for all RPE65 patients with the mean value shown in black. Here, the trajectories of the WM and GM changes over time that have shown the most significant alterations, mainly in the right hemisphere, are being compared. As shown in Fig. 8, while the dendritic arborization (ODI values) of the primary visual cortex increases the microstructural WM (NDI) along the right GS tract declines. Both undergo significant structural changes particularly at 3MO post intervention. The gray matter ODI increases ($p = 0.01$; $p_c = 0.04$; see Table S2) and the white matter NDI decreases ($p = 0.04$; $p_c = 0.16$; see Table S6) as compared with their respective baseline values.

4.7. Longitudinal changes in non-visual gray and white matter control regions

Linear mixed effects model was used to assess the longitudinal ODI measures of the gray matter within the left and right motor cortex as well as the NDI values of the white matter for the left and right anterior limb of the internal capsules (ALIC) (see Fig. S3). The results showed no significant changes in the ODI values for the left ($p = 0.10$), right ($p = 0.89$) and total ($p = 0.83$) motor cortex for the RPE65 patients. Similar analyses showed the same nonsignificant results for changes in the ODI values of the left ($p = 0.36$), right ($p = 0.68$), and total ($p = 0.53$) motor cortex gray matter in sighted control group. The longitudinal changes in the left ($p = 0.07$) and right ($p = 0.10$) NDI values of the ALIC over time in RPE65 patients were also not significant. The analysis of the NDI values of the left ($p = 0.52$) and right ($p = 0.35$) ALIC in the sighted control group also showed no significant changes over time.

5. Discussion

The structural basis and the underlying process of brain plasticity and morphological remodeling of the human visual system in response to vision reversal has predominantly been addressed in animal studies in the context of experience dependent plasticity. The RPE65 clinical trial offered a unique opportunity for an in vivo human model to study and gain a deeper understanding on the process of experience dependent brain plasticity. Here we used an advanced method of magnetic resonance diffusion imaging called Neurite Orientation Dispersion and Density Imaging (NODDI) in a group of RPE65 patients and dynamically monitored neuronal responses of the gray and white matter microstructures within the primary visual system to retinal gene therapy before and 1, 3, 6, and 12 months after vision intervention.

5.1. Effects of retinal gene therapy on dendritic complexity of the primary visual cortex (changes in Brain's gray matter)

Neurons receive and exchange information through their dendritic arbor which is usually highly complex depending on the level of branching and arbor length, two factors that regulate neuronal functions (Solecki et al., 2006). The arbor complexity has been reported to be highly dependent on change in neuronal input with a direct correlation between the degree of enhancement in dendritic complexity and neuronal activity (Redmond et al., 2002; Sin et al., 2002). A clear example of this process is described in (Sin et al., 2002) where increases in visual experience in xenopus laevis tadpoles increased dendritic complexity (Sin et al., 2002). As proposed by Cline (2001), there are two phases of growth and stabilization in neuronal circuit development. In the first phase, which occurs in response to neuronal activity, dendrites and axonal arbors increase in length and branching. In the second phase, the newly formed branches 'check' the environment for optimal synaptic connections (Cline, 2001)and are maintained and stabilized if they form synapses or they are eliminated if the process is unsuccessful (Cline, 2001). Similar data presented by Vaillant et al. (2002) also indicates that neuronal activity promotes dendritic formation and growth. Authors also presented evidence that ongoing activity is required not only for the formation of the dendrites, but also for their maintenance and survival. One genetic factor called "Rem2" has been recently identified as the likely candidate to regulate changes in the dendritic tree in response to neuronal stimulation (Richards et al., 2020). Overall, the balance between dendritic growth and elimination occurs through complex interactions involving neurotransmitters and a number of genes (Ghiretti and Paradis, 2014; Hooks and Chen, 2020; Richards et al., 2020; Sin et al., 2002; Vaillant et al., 2002) and is beyond the context of the present study. However, it is the balance between these two processes that is important to the final improvement of neuronal structures in response to external stimulation (Ghiretti and Paradis, 2014).

Collectively, prior work on normal development or sensory experience dependent dendritic changes suggests that there exists an initial phase of rapid dendritic growth which at some point is limited in degree of branching and length increase. This activity and experience dependent neural plasticity have been shown not to be limited to an early development and sensitivity period, but to continue into adulthood as well (Ghiretti and Paradis, 2014; Hooks and Chen, 2020).

Consistent with previous animal studies, after retinal gene therapy (and presumably due to improved vision) we observed an initial increase in the ODI of the primary visual cortex, primarily within the inferior pericalcarine tissue. However, this increase in the ODI did not continue indefinitely and at some timepoint (3-months post intervention), the average total inferior ODI value reached its maximum value and started to decline (see Fig. 3B). According to Richards and colleagues (Richards et al., 2020) dendritic complexity of the visual cortex in response to visual experience and normal development is regulated by genetic factors (Richards et al., 2020) that act to both promote and at the same time restrict dendritic growth. An earlier work (Ghiretti and Paradis, 2014) also reported that, while visual experience promotes dendritic complexity, there is a mechanism that controls dendritic arborization in order to ensure that growth-promoting processes stay checked (Ghiretti and Paradis, 2014). Consistent with these findings, our preliminary results also indicate an initial phase with highly dynamic dendritic arbor development in response to visual experience prompted by retinal gene therapy, and a second phase of decline to a stabilized level, perhaps through previously described processes of arbor retractions, synaptogenesis, and pruning (Cline, 2001). As presented in Table 3, the one year follow up of the ODI measures of the same primary visual cortex areas in a group of sighted controls did not present with significant changes in the dendritic distribution over time.

The data on the actual timing or the exact trajectory of the changes in dendritic complexity particularly from sensory stimulation is scarce. However, a recent review (Elston and Fujita, 2014) on animal and human postnatal spinogenesis of the dendritic and axonal growth reports that pyramidal cell development in the brain takes place at different rates for different brain areas. During the past decades, there have been two prevalent theories on postnatal synaptogenesis (Elston and Fujita, 2014). One suggested by Rakic et al. (1986) states that in the macaque monkey maximum synaptic connectivity is achieved at around 3.5 months of age for all brain areas and after that there will be a net reduction in the number of synaptic connections all over the cortex (see Fig. 1 in (Elston and Fujita, 2014)). The other theory by Huttenlocher and Dabholkar (Huttenlocher and Dabholkar, 1997) who studied the human brain, proposed that different cortical areas mature at different rates and time points after birth. However, the timing for the visual cortex development for maximum synapses was reported to occur at 3 months after birth (see Fig. 2 in (Elston and Fujita, 2014)). Thus,

regardless of the different theories, the timing for the peak of postnatal synaptogenesis for the visual cortex was reported to be around 3–3.5 months.

It is not yet clear whether the trajectory and process of experience dependent brain development follows those proposed for postnatal development. However, in the current study, the effect of visual experience prompted by retinal gene therapy on the dendritic tree of the primary visual cortex showed a similar timing (3 months post intervention; see Fig. 3B) for the peak dendritic changes which is consistent with the timing for the peak synaptogenesis of the visual cortex proposed by two different postnatal brain development theories (Huttenlocher and Dabholkar, 1997; Rakic et al., 1986).

5.2. Correlations between patients' FST response and dendritic complexity of the primary visual cortex

Association between the total inferior and superior pericalcarine tissue dendritic distribution and the patients' FST clinical measures for all time points are presented in Figs. 5 and 6 respectively. Note that the lower FST values correspond to a higher ocular function. Therefore, a negative correlation between the FST and the ODI measures means that a higher ODI value correlates with a more sensitive FST response, and a positive correlation means that a lower ODI value correlates with higher patient sensitivity to FST stimuli. As shown in Table S2, the most significant correlations were observed for the inferior pericalcarine gray matter measures and the blue and white color FST responses for both the left and the right eyes, particularly at 3MO. Although, the left eye also showed significant correlations at 6 and 12 months for the white color FST stimuli after retinal intervention and the right eye at 6MO for the blue FST responses. The lack of significant correlations of the inferior pericalcarine gray matter to the red stimuli is consistent with the patients' lower sensitivity to the red color FST stimuli (see Fig. 4) as compared to the blue and white FST responses. Interestingly, we did not observe any significant correlations for either the left or right eye FST responses and the total superior calcarine tissue (see Table S3). The negative correlations for the ODI values of the total inferior pericalcarine gray matter with the FST responses are suggestive of the fact that increases in dendritic population may corresponds to stronger FST responses, particularly at 3MO time point, when maximum dendritic dispersion occurs.

5.3. 5.3. effects of retinal gene therapy on the geniculostriate pathway (changes in Brain's white matter)

Experience dependent brain plasticity is hypothesized to affect both the gray and white matter components of the visual pathway, and the white matter especially plays a pivotal role in this process (Fields, 2020). The main white matter fiber bundle that relays more than 90% of the visual information to the primary visual cortex is the GS pathway. The longitudinal changes in the neurite density index (NDI) of the left and right GS tracts are presented in Fig. 6. In general, normal development or the experience dependent changes in the brain's white matter over time is expected to manifest as an asymptotic increase in axonal myelination (increased NDI) over time (Chang et al., 2015; Genc et al., 2017). This is reflected in the NDI values of the left and right GS tracks for the sighted controls shown in Table 3. As depicted in Table 3, the average NDI value along the left GS tract among controls increased from 0.57 (at baseline) to 0.60 (at 1 YR) and for the right tract it increased from 0.55 (at Baseline) to 0.58 (at 1 YR), an approximately 5% increase in the NDI value. On the other hand, the overall the NDI increase over one year for the RPE65 patients was from 0.56 (at baseline) to 0.57 (at 1 YR) which is less than 2%, which is 50% less than expected value of matched controls. The lack of expected NDI increase along the GS tract in patients could be attributed to an initial decrease in axonal myelination and transition through the lowest NDI value at 3 MO. Thus, despite the expected continuous increase in axonal myelination, after retinal intervention, the NDI values of the GS tracts started to decline reaching a minimum at 3MO post treatment and then began to ascend and continued to grow to above of their baseline value at one year after sight restoration. The trajectory of the WM changes along the GS tracts was the opposite of the observed ODI (gray matter) changes of the primary visual cortex (see Fig. 3). While both the right and left GS tracts showed an analogous trajectory over time with a similar dip at 3MO, only the changes in the right GS tract reached overall statistical significance ($p < 0.03$). Interestingly, the right dominant laterality observed for the neurite density along the GS tracts was consistent with the laterality observed in dendritic changes within the primary visual cortex. Furthermore, the unexpected statistically significant abrupt trajectory changes observed for both the neurite density of the GS tracts and the dendritic distribution within the primary visual cortex occurred exactly at 3MO after retinal intervention.

While increases in white matter or axonal myelination have been considered a gold standard outcome measure for brain plasticity (Purger et al., 2016), recent studies are now proposing transmission timing of neuronal impulses as the key factor for learning and development (Dutta et al., 2018). Although, the two are tightly related as the optimal impulse transmission speeds are regulated by the degree of neural myelination (Fields, 2020; Fields and Dutta, 2019). Thus, the myelin that has been already formed on an axon needs to be thickened to increase transmission speed or thinned to slow signal transmission (Fields, 2020; Fields and Dutta, 2019). Therefore, myelin structure that once was considered static is now proposed to be a dynamic process which thickens by adding layers next to the axon by the oligodendrocytes and thins by removing layers from the outer sheath through a controlled process by the astrocytes (Dutta et al., 2018). The cellular processes of the axonal myelination or demyelination to establish optimal transmission speed within a neuronal circuit takes place in an elaborate manner involving the neurotransmitters, oligodendrocytes, glial and astrocyte cells, and various enzymes etc. And are described in detail elsewhere (Dutta et al., 2018; Fields and Dutta, 2019).

Based on the newly proposed hypothesis that axonal myelin is not just thinned due to disease but can dynamically change under normal conditions to adjust for an optimal signal transmission time, we assume that the initial decrease in neural density index (NDI) values of the GS tracts might be due to the myelin thinning process in an attempt to optimize transmission timing of the visual signals. We hypothesize that synaptic connections made by the newly formed dendritic arbors within the primary visual areas are thin, unmyelinated/somewhat myelinated connections and are unable to process high speed signals transmitted along a thicker myelinated axon. Therefore, signal transmission must be adjusted such that the visual signals are synchronized to arrive at the same speed/time as the one being fired by the newly developed connections. As such, the transmission speed along the GS tracts would need to be reduced. To slow down the transmission speed of the visual signals for a timely arrival to the primary visual cortex, the myelination around the GS tracts must be thinned. The thinning process will synchronize the arrival time of the visual signals to an optimal processing level by the newly formed dendritic connection within the primary visual areas. The trajectory of change along the GS tracts is hypothesized to follow an opposite path of the development for the dendritic trees within the pericalcarine tissue. Once the dendritic population reaches a maximum and start its decline, the axonal myelination also reaches a minimum and starts to climb and continue to increase to retain optimal signal transmission time.

5.4. Correlations between patients' FST response and neurite density along the geniculostriate pathway

The correlations between the patients' FST clinical measures for the right and left eyes and the neurite density (NDI) along the right and left GS tracks for baseline and all time points post intervention are presented in Fig. 7. As presented in Tables S4 and S5, the most significant

correlations between the NDI values of the GS tracks and FST measures occurred at baseline and 3MO time point, primarily for the blue and white color stimuli. Consistent with the results from the correlations between the dendritic growth and FST responses, these results also show that RPE65 patients were most sensitive to the blue and white color FST stimuli and less sensitive to the red FST stimulus. Note that for both the left and right GS tracks, negative correlations were observed at baseline between the NDI and FST values, indicating that patients with higher NDI values show larger FST responses. Whereas the same correlations at 3MO time points were positive and showing the opposite association. In other words, as is normally expected, the higher neural density for the GS tracks at baseline indicated better FST responses. However, at 3MO post intervention, the opposite was observed, and lower neural density along the GS tracts had better patient FST responses. Furthermore, we also observed negative correlations between the ODI of the total inferior calcarine tissue and the FST responses suggesting an increase in dendritic tree corresponds to higher FST responses, particularly at 3MO time point. Thus, while increases in the population of dendrites showed better FST responses, the opposite correlations were observed for the NDI values of the GS tracks. These results further support the idea for myelin thinning processes to slow down the neuronal processing speed to optimize signal processing for the synaptic connections of the newly formed dendritic trees.

5.5. Longitudinal structural changes in non-visual control regions

Two areas outside the visual system representing the brain's gray and white matter were selected to act as non-visual control regions. The changes in the NODDI indices, such as ODI or NDI, of these areas were assessed over time to examine whether they followed the same trajectory of change over time, as was observed for the visual areas. For the gray matter, a portion of the left and right motor cortex and for the white matter the left and right anterior limb of the internal capsule (ALIC) were selected. Results showed that while significant changes in the ODI values of the primary visual cortex for the RPE65 patients were detected, no changes in the gray matter of the motor cortex were observed for neither the patients nor the sighted controls. Similar findings were observed for the NDI values of the WM control regions. Therefore, changes observed within the visual areas can be considered more specific to the retinal gene therapy responses. Although, retinal gene therapy may affect other brain regions causing other functional enhancements, such as increases in mobility (Maguire et al., 2019; Russell et al., 2017) but that may not be considered a direct effect.

5.6. Laterality of changes within the visual system

Significant changes for the gray and white matter of the visual structures and their correlations with the patients' FST responses after gene therapy were primarily detected on the right hemisphere. This detected laterality was an unexpected finding as all the patients received treatment to both eyes. The RPE65 patients were injected bilaterally, first to their worse seeing eyes (6/9 in the left eye) and within 6–18 days they received a second injection to the untreated contralateral eye (Russell et al., 2017). The subretinal injections were generally delivered to the superior and nasal aspects of the fovea, approximately two disk (optic disk diameter) areas distant from the foveal center (to minimize stress on this vulnerable tissue)(Maguire et al., 2019, 2021; Russell et al., 2017). Considering that both eyes were injected within one or two weeks, equal bilateral hemispheric changes in both the gray and white matter were predicted. Based on our previously reported results from the earlier RPE65 Phase 1 Clinical Trial patients (Ashtari et al., 2015), we believe that the subretinal delivery of the vector genome normally stays local to the injection site and dose not spread laterally along the retina. For example, if the injection is delivered to the temporal location, it would not spread to the nasal retinal areas. Also, the location of the subretinal injection has great influences on the downstream effects observed on the visual cortex. For instance, the findings from our previous diffusion study in a group of patients from Phase 1 Clinical Trial, who received subretinal injections to their right superior temporal retina (9/10 injected in the right eye), showed significant myelination of the right GS tract and not the left (Ashtari et al., 2015). This may be because the axons from the temporal ganglion cells stay ipsilaterally and the ones from the nasal retina cross to the contralateral hemisphere (Aebersold et al., 1981; Purves, 2001). Consequently, for the Phase 3 Clinical Trial patients who received their subretinal injection to their superior nasal retinal locations, we hypothesized to observe a downstream effect to the contralateral visual cortex (nasal fibers cross to the contralateral hemisphere). As such, subretinal injection to the left eye would affect the right visual cortex and vice versa. Here the Phase 3 patients, unlike the Phase 1patients, received bilateral gene therapy and the effects of their subretinal injections must have been observed bilaterally within the right and left visual cortices. However, structural changes within the visual system were mainly significant for the right side which is mainly reflective of the first eye injection (6/9 first injected in the superior nasal location of the left eye where the fibers cross to the contralateral hemisphere) and the effects from the second eye injection (6/9 received second injection in the superior nasal location of the right eye) seemed to be very slight and at a trend level (see Tables 2 and 3). The right sided laterality effects were unexpectedly shared for both the ODI of the primary visual cortex and the NDI of the GS tracts. While the consistency in these results is reassuring, we have no clear explanation for the observed strong right sided laterality. The process, however, may be similar to the process of competition for ocular dominance during brain development (Harris et al., 1997)and is suggestive of some form of rivalry for brain plasticity within the visual cortex that could be in competition with the contralateral brain normalization process. As this explanation is purely speculative more careful studies are warranted to address this important question.

5.7. Superior vs inferior dendritic changes of the primary visual cortex

In addition to the temporal and nasal division along the horizontal direction, the retinal surface is also divided into superior and inferior sections in the vertical direction (Aebersold et al., 1981). The superior retina corresponds to the superior calcarine tissue and the inferior retina to the inferior calcarine areas. While there is a one to one relationship between the retina and the calcarine tissues (Aebersold et al., 1981), they both correspond to the opposite visual fields. For example, both the superior retina and calcarine tissue correlate with the patients' inferior visual field and vice versa. The gene augmentation therapy surgery is targeted to the superior retina to increase the inferior aspect of the visual field in the RPE65 patients. As such, we expected to detect the most significant changes along the superior calcarine tissue. However, analyses of the ODI values showed significant longitudinal changes to occur along the inferior pericalcarine tissue with minimal alteration within the superior calcarine areas. One explanation for this unexpected result is that the subretinal injected material could in fact diffuse to the inferior retina just due to gravitational forces. Another reason is perhaps the retinal detachment resulting from the subretinal injection within the superior retinal could have expanded to expose the inferior areas of the retina as well. The surgeon at the CHOP site (AM) performing the surgical procedures on almost all the RPE65 patients stated that "The bleb generated by the subretinal injection can drift" (personal communication). In fact, immediately following the subretinal injection, all subjects' heads were positioned so that if the bleb were to expand, gravity would expand the bleb in the inferior direction. Monitoring the expansion of the bleb immediately post injection would generally requires prolonged anesthesia which is not in the patients' best interest. Also, since the retina usually reattaches within 24 h a long-term follow-up was also not helpful in localizing the bleb. Therefore, based on the neuroimaging results and due to the expansion/drift/diffusion of the bleb in the hours or days post-surgery, the superior injection site noted in the

operating reports doesn't necessarily indicate that ultimately only superior retina was exposed.

5.8. Pitfalls of longitudinal change in gray and white matter at 3MO

The observed changes at 3MO post-baseline may well be a direct result of the therapeutic intervention and resulting changes in visual sensitivity. However, the observed change may also be a result of other effects such as scanner drift or changes in subject motion. Although, in the control regions of interest - the motor cortex and the anterior limb of the internal capsule - no significant differences were observed over time and at 3MO compared to baseline. In general, scanner drift may include gradual changes between scanner calibration events, system software upgrades, hardware repairs, or changes in operating procedures. However, we believe scanner drift is unlikely to account for the observed changes mainly since the timing of the 3MO visit for each subject was dispersed over a period of fourteen months, as shown in Fig. S5. Another factor that is well known to introduce biases in diffusion measures (Roalf et al., 2016) is the participant head motion during the diffusion scans. We used FSL's eddy to estimate and correct participant head motion (Andersson and Sotiropoulos, 2016). Eddy estimates the relative framewise displacement (FWD), in mm, of all voxels within the brain mask, for each diffusion-weighted volume. We analyzed the motion data with the longitudinal mixed-effects model we used for the DTI and NODDI measures. As depicted in Table S7 no significant motions were observed over time in patients, and a post-hoc test comparing motion at 3MO to baseline was also not significant. Analyses of the motion data in sighted controls also showed no significant motion between the baseline and 1 YR visits of sighted controls (see Table S8). Therefore, these data suggest that the observed overall changes in the visual GM and WM over time and at 3MO time point are not the result of global changes caused by scanner drifts or subject motion.

The current study involves a unique cohort of patients that is rare to obtain with large number of participants. Due to the small sample size, the statistical comparisons were performed with and without correction for multiple comparisons. After corrected for multiple comparisons, while some comparisons remained significant many did not or became borderline significant. Future studies with larger number of participants are needed to replicate current study findings.

6. Summary and conclusions

Expanding our understanding of the underlying mechanisms leading to human brain plasticity has been among the main goals of the neuroscience community. In reaching this goal, studies of the human sensory systems, and in particular the visual pathway, have always played a pivotal role. However, much of our current knowledge on the process of brain plasticity in the visual systems stems from animal studies. Having access to a unique group of patients who gained sight through retinal gene therapy has provided a powerful human model to dynamically examine the underlying processes for brain plasticity through analyzing the changes of the brain's gray and white matter before and after intervention. The dynamic changes of the brain were captured through advanced methods of magnetic resonance imaging at baseline, 1MO, 3MO, 6MO, and 12MO after retinal intervention. Consistent with previous animal studies, and in response to vision restoration, we observed an initial growth in the dendritic arborization (gray matter) of the primary visual cortex that peaked at 3 MO post intervention, which is similar to the timing reported for the peak synaptogenesis of the visual cortex proposed by two different postnatal brain development theories (Huttenlocher and Dabholkar, 1997; Rakic et al., 1986). The white matter changes were evaluated along the GS tracts (optic radiation), which is the main fiber bundle transferring the visual information to the primary visual cortex. Traditionally, experience dependent brain plasticity is manifested as an increase in myelination along these tracts (Ashtari et al., 2015; Paul et al., 2014). However, evaluation of the dynamic changes of the white matter along these tracts shows that before an increase in myelination can occur, the axonal myelin undergoes thinning (demyelination). This result is in line with recent animal studies elucidating axonal demyelination as a new brain plasticity process (Dutta et al., 2018; Fields and Dutta, 2019).

In conclusion, our results demonstrate that reorganization of brain structures in response to vision restoration is a dynamic process with the largest brain alteration occurring at 3MO post intervention. The study reveals -an unexpected finding -that the initial brain response to reinstating vision may in fact start with a demyelination process of the axonal fibers carrying visual information to the primary visual cortex. The expected increase in myelination follows once the newly established dendrites undergo population decrease through apoptosis and synaptogenesis. This study also illustrates the power of advanced magnetic resonance method of NODDI in assessing the in vivo dynamic changes of tissue microstructures in human in response to vision restoration. Finally, there is growing evidence for brain changes through training reported in several cross-sectional and longitudinal studies in humans (Bengtsson et al., 2005; Scholz et al., 2009; Taubert et al., 2010). Based on these reports, it may also be possible to augment the brain changes prompted by the retinal gene therapy through targeted vision rehabilitation programs. According to our preliminary results, administration of a vision rehab program may be most effective within the first three months of retinal intervention. Future studies are warranted to replicate these results and assess the efficacy of targeted vision rehabilitation programs following retinal intervention to reinstate or preserve vision.

Funding information

This study was supported by the National Eye Institute (grant number: R01EY025287-01A1) and the Center for Advanced Retinal and Ocular Therapeutics (CAROT) at the University of Pennsylvania Perelman School of Medicine, research to prevent blindess (RPB) Foundation, and the F.M. Kirby Foundation.

CRediT authorship contribution statement

Manzar Ashtari: conceived, designed, and implemented the idea, and wrote the manuscript, provided the funding source for the study. **Philip Cook:** performed all related image pre and post processing and analyses. **Mikhail Lipin:** performed all related image pre and post processing and analyses. **Yinxi Yu:** performed statistical analysis of the data and interpretation of the results. **Gui-Shuang Ying:** performed statistical analysis of the data and interpretation of the results. **Albert Maguire:** performed the subretinal administration for retinal gene therapy, performed all patients' FST clinical measures, Again, all authors contributed to reviewing/editing of the manuscript. **Jean Bennett:** provided the funding source for the study, performed all patients' FST clinical measures. **James Gee:** supervised the use of all the software used for image analyses. **Hui Zhang:** supervised the use of all the software used for image analyses.

Declaration of competing interest

The authors declare that they have no known competing financial interests or personal relationships that could have appeared to influence the work reported in this paper.

Data availability

Data will be made available on request.

Acknowledgements

We would like to express our special gratitude to Dr. Holly Bridge from the Oxford University for taking the time to review and edit this

manuscript and her wonderful constructive suggestions. We also would like to thank Dr. Douglas Fields from the National Institute of Health for his expert opinion, guidance, and helpful scientific discussions.

Appendix A. Supplementary data

Supplementary data to this article can be found online at https://doi.org/10.1016/j.crneur.2023.100089.

References

Adluru, G., Gur, Y., Anderson, J.S., Richards, L.G., Adluru, N., DiBella, E.V., 2014. Assessment of white matter microstructure in stroke patients using NODDI. In: 2014 36th Annual International Conference of the IEEE Engineering in Medicine and Biology Society. IEEE, pp. 742–745.

Aebersold, H., Creutzfeldt, O.D., Kuhnt, U., Sanides, D., 1981. Representation of the visual field in the optic tract and optic chiasma of the cat. Exp. Brain Res. 42, 127–145.

Andersson, J.L., Sotiropoulos, S.N., 2016. An integrated approach to correction for off-resonance effects and subject movement in diffusion MR imaging. Neuroimage 125, 1063–1078.

Andica, C., Kamagata, K., Hatano, T., Okuzumi, A., Saito, A., Nakazawa, M., Ueda, R., Motoi, Y., Kamiya, K., Suzuki, M., 2018. Neurite orientation dispersion and density imaging of the nigrostriatal pathway in Parkinson's disease: retrograde degeneration observed by tract-profile analysis. Parkinsonism & related disorders 51, 55–60.

Andica, C., Kamagata, K., Hayashi, T., Hagiwara, A., Uchida, W., Saito, Y., Kamiya, K., Fujita, S., Akashi, T., Wada, A., Abe, M., Kusahara, H., Hori, M., Aoki, S., 2020. Scan–rescan and inter-vendor reproducibility of neurite orientation dispersion and density imaging metrics. Neuroradiology 62, 483–494.

Ashtari, M., Cyckowski, L.L., Monroe, J.F., Marshall, K.A., Chung, D.C., Auricchio, A., Simonelli, F., Leroy, B.P., Maguire, A.M., Shindler, K.S., 2011. The human visual cortex responds to gene therapy–mediated recovery of retinal function. J. Clin. Invest. 121, 2160–2168.

Ashtari, M., Nikonova, E.S., Marshall, K.A., Young, G.J., Aravand, P., Pan, W., Ying, G.-s., Willett, A.E., Mahmoudian, M., Maguire, A.M., 2017. The role of the human visual cortex in assessment of the long-term durability of retinal gene therapy in follow-on RPE65 clinical trial patients. Ophthalmology 124, 873–883.

Ashtari, M., Zhang, H., Cook, P.A., Cyckowski, L.L., Shindler, K.S., Marshall, K.A., Aravand, P., Vossough, A., Gee, J.C., Maguire, A.M., 2015. Plasticity of the human visual system after retinal gene therapy in patients with Leber's congenital amaurosis. Sci. Transl. Med. 7, 296ra110-296ra110.

Baroncelli, L., Lunghi, C., 2021. Neuroplasticity of the visual cortex: in sickness and in health. Exp. Neurol. 335, 113515.

Bengtsson, S.L., Nagy, Z., Skare, S., Forsman, L., Forssberg, H., Ullén, F., 2005. Extensive piano practicing has regionally specific effects on white matter development. Nat. Neurosci. 8, 1148–1150.

Bennett, J., Ashtari, M., Wellman, J., Marshall, K.A., Cyckowski, L.L., Chung, D.C., McCague, S., Pierce, E.A., Chen, Y., Bennicelli, J.L., 2012. AAV2 gene therapy readministration in three adults with congenital blindness. Sci. Transl. Med. 4, 120ra115-120ra115.

Bennett, J., Wellman, J., Marshall, K.A., McCague, S., Ashtari, M., DiStefano-Pappas, J., Elci, O.U., Chung, D.C., Sun, J., Wright, J.F., 2016. Safety and durability of effect of contralateral-eye administration of AAV2 gene therapy in patients with childhood-onset blindness caused by RPE65 mutations: a follow-on phase 1 trial. Lancet 388, 661–672.

Castaldi, E., Lunghi, C., Morrone, M.C., 2020. Neuroplasticity in adult human visual cortex. Neurosci. Biobehav. Rev. 112, 542–552.

Chang, Y.S., Owen, J.P., Pojman, N.J., Thieu, T., Bukshpun, P., Wakahiro, M.L., Berman, J.I., Roberts, T.P., Nagarajan, S.S., Sherr, E.H., Mukherjee, P., 2015. White matter changes of neurite density and fiber orientation dispersion during human brain maturation. PLoS One 10, e0123656.

Chen, J.L., Lin, W.C., Cha, J.W., So, P.T., Kubota, Y., Nedivi, E., 2011. Structural basis for the role of inhibition in facilitating adult brain plasticity. Nat. Neurosci. 14, 587–594.

Chung, A.W., Seunarine, K.K., Clark, C.A., 2016. NODDI reproducibility and variability with magnetic field strength: a comparison between 1.5 T and 3 T. Hum. Brain Mapp. 37, 4550–4565.

Cline, H.T., 2001. Dendritic arbor development and synaptogenesis. Curr. Opin. Neurobiol. 11, 118–126.

Colgan, N., Siow, B., O'Callaghan, J.M., Harrison, I.F., Wells, J.A., Holmes, H.E., Ismail, O., Richardson, S., Alexander, D.C., Collins, E.C., 2016. Application of neurite orientation dispersion and density imaging (NODDI) to a tau pathology model of Alzheimer's disease. Neuroimage 125, 739–744.

Dutta, D.J., Woo, D.H., Lee, P.R., Pajevic, S., Bukalo, O., Huffman, W.C., Wake, H., Basser, P.J., SheikhBahaei, S., Lazarevic, V., 2018. Regulation of myelin structure and conduction velocity by perinodal astrocytes. Proc. Natl. Acad. Sci. USA 115, 11832–11837.

Elston, G.N., Fujita, I., 2014. Pyramidal cell development: postnatal spinogenesis, dendritic growth, axon growth, and electrophysiology. Front. Neuroanat. 8, 78.

Fields, R.D., 2020. The Brain Learns in Unexpected Ways: neuroscientists have discovered a set of unfamiliar cellular mechanisms for making fresh memories. Sci. Am. 322, 74.

Fields, R.D., Dutta, D.J., 2019. Treadmilling model for plasticity of the myelin sheath. Trends Neurosci. 42, 443–447.

Genc, S., Malpas, C.B., Holland, S.K., Beare, R., Silk, T.J., 2017. Neurite density index is sensitive to age related differences in the developing brain. Neuroimage 148, 373–380.

Ghiretti, A.E., Paradis, S., 2014. Molecular mechanisms of activity-dependent changes in dendritic morphology: role of RGK proteins. Trends Neurosci. 37, 399–407.

Harris, A.E., Ermentrout, G.B., Small, S.L., 1997. A model of ocular dominance column development by competition for trophic factor. Proc. Natl. Acad. Sci. USA 94, 9944–9949.

Hochberg, Y.A., 1988. A sharper Bonferroni procedure for multiple significance testing. Biometrika 75, 3.

Holtmaat, A., Wilbrecht, L., Knott, G.W., Welker, E., Svoboda, K., 2006. Experience-dependent and cell-type-specific spine growth in the neocortex. Nature 441, 979–983.

Hooks, B.M., Chen, C., 2020. Circuitry underlying experience-dependent plasticity in the mouse visual system. Neuron 106, 21–36.

Huttenlocher, P.R., Dabholkar, A.S., 1997. Regional differences in synaptogenesis in human cerebral cortex. J. Comp. Neurol. 387, 167–178.

Jacobson, S.G., Cideciyan, A.V., Ratnakaram, R., Heon, E., Schwartz, S.B., Roman, A.J., Peden, M.C., Aleman, T.S., Boye, S.L., Sumaroka, A., 2012. Gene therapy for leber congenital amaurosis caused by RPE65 mutations: safety and efficacy in 15 children and adults followed up to 3 years. Arch. Ophthalmol. 130, 9–24.

Jin, M., Li, S., Moghrabi, W.N., Sun, H., Travis, G.H., 2005. Rpe65 is the retinoid isomerase in bovine retinal pigment epithelium. Cell 122, 449–459.

Kamagata, K., Hatano, T., Okuzumi, A., Motoi, Y., Abe, O., Shimoji, K., Kamiya, K., Suzuki, M., Hori, M., Kumamaru, K.K., 2016. Neurite orientation dispersion and density imaging in the substantia nigra in idiopathic Parkinson disease. Eur. Radiol. 26, 2567–2577.

Kamiya, K., Hori, M., Aoki, S., 2020. NODDI in clinical research. J. Neurosci. Methods 346, 108908.

Kirkwood, A., Bear, M.F., 1994. Hebbian synapses in visual cortex. J. Neurosci. 14, 1634–1645.

Kraguljac, N.V., Guerreri, M., Strickland, M.J., Zhang, H., 2022. Neurite orientation dispersion and density imaging in psychiatric disorders: a systematic literature review and a technical note. Biol. Psychiatr. Glob. Open Sci. 3 (1), 10–21. January 2022.

Krieger, P., 2009. Experience-dependent increase in spine calcium evoked by backpropagating action potentials in layer 2/3 pyramidal neurons in rat somatosensory cortex. Eur. J. Neurosci. 30, 1870–1877.

Laird, N.M., Ware, J.H., 1982. Random-effects Models for Longitudinal Data. Biometrics, pp. 963–974.

Lehmann, N., Aye, N., Kaufmann, J., Heinze, H.-J., Düzel, E., Ziegler, G., Taubert, M., 2021. Longitudinal reproducibility of neurite orientation dispersion and density imaging (NODDI) derived metrics in the white matter. Neuroscience 457, 165–185.

Lendvai, B., Stern, E.A., Chen, B., Svoboda, K., 2000. Experience-dependent plasticity of dendritic spines in the developing rat barrel cortex in vivo. Nature 404, 876–881.

Lunghi, C., Galli-Resta, L., Binda, P., Cicchini, G.M., Placidi, G., Falsini, B., Morrone, M. C., 2019. Visual cortical plasticity in retinitis pigmentosa. Invest. Ophthalmol. Vis. Sci. 60, 2753–2763.

Maguire, A.M., High, K.A., Auricchio, A., Wright, J.F., Pierce, E.A., Testa, F., Mingozzi, F., Bennicelli, J.L., Ying, G.-s., Rossi, S., 2009. Age-dependent effects of RPE65 gene therapy for Leber's congenital amaurosis: a phase 1 dose-escalation trial. Lancet 374, 1597–1605.

Maguire, A.M., Russell, S., Chung, D.C., Yu, Z.-F., Tillman, A., Drack, A.V., Simonelli, F., Leroy, B.P., Reape, K.Z., High, K.A., 2021. Durability of voretigene neparvovec for biallelic RPE65-mediated inherited retinal disease: phase 3 results at 3 and 4 years. Ophthalmology 128, 1460–1468.

Maguire, A.M., Russell, S., Wellman, J.A., Chung, D.C., Yu, Z.-F., Tillman, A., Wittes, J., Pappas, J., Elci, O., Marshall, K.A., 2019. Efficacy, safety, and durability of voretigene neparvovec-rzyl in RPE65 mutation–associated inherited retinal dystrophy: results of phase 1 and 3 trials. Ophthalmology 126, 1273–1285.

Maguire, A.M., Simonelli, F., Pierce, E.A., Pugh Jr., E.N., Mingozzi, F., Bennicelli, J., Banfi, S., Marshall, K.A., Testa, F., Surace, E.M., 2008. Safety and efficacy of gene transfer for Leber's congenital amaurosis. N. Engl. J. Med. 358, 2240–2248.

Majewska, A., Sur, M., 2003. Motility of dendritic spines in visual cortex in vivo: changes during the critical period and effects of visual deprivation. Proc. Natl. Acad. Sci. USA 100, 16024–16029.

Mataga, N., Mizuguchi, Y., Hensch, T.K., 2004. Experience-dependent pruning of dendritic spines in visual cortex by tissue plasminogen activator. Neuron 44, 1031–1041.

Matsuzaki, M., Honkura, N., Ellis-Davies, G.C., Kasai, H., 2004. Structural basis of long-term potentiation in single dendritic spines. Nature 429, 761–766.

Medini, P., 2014. Experience-dependent plasticity of visual cortical microcircuits. Neuroscience 278, 367–384.

Moiseyev, G., Chen, Y., Takahashi, Y., Wu, B.X., Ma, J.X., 2005. RPE65 is the isomerohydrolase in the retinoid visual cycle. Proc. Natl. Acad. Sci. U. S. A. 102, 12413–12418.

Mori, s., Wakana, S., Nagae, L., 2005. MRI Atlas of the Human White Matter.

Nazeri, A., Chakravarty, M.M., Rotenberg, D.J., Rajji, T.K., Rathi, Y., Michailovich, O.V., Voineskos, A.N., 2015. Functional consequences of neurite orientation dispersion and density in humans across the adult lifespan. J. Neurosci. 35, 1753–1762.

Noguchi, J., Matsuzaki, M., Ellis-Davies, G.C., Kasai, H., 2005. Spine-neck geometry determines NMDA receptor-dependent Ca2+ signaling in dendrites. Neuron 46, 609–622.

Oray, S., Majewska, A., Sur, M., 2004. Dendritic spine dynamics are regulated by monocular deprivation and extracellular matrix degradation. Neuron 44, 1021–1030.
Palacios, E.M., Owen, J.P., Yuh, E.L., Wang, M.B., Vassar, M.J., Ferguson, A.R., Diaz-Arrastia, R., Giacino, J.T., Okonkwo, D.O., Robertson, C.S., Stein, M.B., Temkin, N., Jain, S., McCrea, M., MacDonald, C.L., Levin, H.S., Manley, G.T., Mukherjee, P., 2020. The evolution of white matter microstructural changes after mild traumatic brain injury: a longitudinal DTI and NODDI study. Sci. Adv. 6, eaaz6892.
Parvathaneni, P., Nath, V., Blaber, J.A., Schilling, K.G., Hainline, A.E., Mojahed, E., Anderson, A.W., Landman, B.A., 2018. Empirical reproducibility, sensitivity, and optimization of acquisition protocol, for Neurite Orientation Dispersion and Density Imaging using AMICO. Magn. Reson. Imag. 50, 96–109.
Paul, D.A., Gaffin-Cahn, E., Hintz, E.B., Adeclat, G.J., Zhu, T., Williams, Z.R., Vates, G.E., Mahon, B.Z., 2014. White matter changes linked to visual recovery after nerve decompression. Sci. Transl. Med. 6, 266ra173.
Purger, D., Gibson, E.M., Monje, M., 2016. Myelin plasticity in the central nervous system. Neuropharmacology 110, 563–573.
Purves, D., Augustine, G.J., Fitzpatric, D., et al., 2001. The Midline Sagittal Surface of the Brain, second ed. Sinauer Associates: Neuroscience, Sunderland (MA).
Rae, C.L., Davies, G., Garfinkel, S.N., Gabel, M.C., Dowell, N.G., Cercignani, M., Seth, A. K., Greenwood, K.E., Medford, N., Critchley, H.D., 2017. Deficits in neurite density underlie white matter structure abnormalities in first-episode psychosis. Biol. Psychiatr. 82, 716–725.
Rakic, P., Bourgeois, J.-P., Eckenhoff, M.F., Zecevic, N., Goldman-Rakic, P.S., 1986. Concurrent overproduction of synapses in diverse regions of the primate cerebral cortex. Science 232, 232–235.
Redmond, L., Kashani, A.H., Ghosh, A., 2002. Calcium regulation of dendritic growth via CaM kinase IV and CREB-mediated transcription. Neuron 34, 999–1010.
Richards, S.E., Moore, A.R., Nam, A.Y., Saxena, S., Paradis, S., Van Hooser, S.D., 2020. Experience-dependent development of dendritic arbors in mouse visual cortex. J. Neurosci. 40, 6536–6556.
Roalf, D.R., Quarmley, M., Elliott, M.A., Satterthwaite, T.D., Vandekar, S.N., Ruparel, K., Gennatas, E.D., Calkins, M.E., Moore, T.M., Hopson, R., 2016. The impact of quality assurance assessment on diffusion tensor imaging outcomes in a large-scale population-based cohort. Neuroimage 125, 903–919.
Roman, A.J., Schwartz, S.B., Aleman, T.S., Cideciyan, A.V., Chico, J.D., Windsor, E.A., Gardner, L.M., Ying, G.-s., Smilko, E.E., Maguire, M.G., 2005. Quantifying rod photoreceptor-mediated vision in retinal degenerations: dark-adapted thresholds as outcome measures. Exp. Eye Res. 80, 259–272.
Roman, A.J., Cideciyan, A.V., Wu, V., Garafalo, A.V., Jacobson, S.G., 2022. Full-field stimulus testing: role in the clinic and as an outcome measure in clinical trials of severe childhood retinal disease. Prog. Retin. Eye Res. 87, 101000.
Russell, S., Bennett, J., Wellman, J.A., Chung, D.C., Yu, Z.-F., Tillman, A., Wittes, J., Pappas, J., Elci, O., McCague, S., 2017. Efficacy and safety of voretigene neparvovec (AAV2-hRPE65v2) in patients with RPE65-mediated inherited retinal dystrophy: a randomised, controlled, open-label, phase 3 trial. Lancet 390, 849–860.
Scholz, J., Klein, M.C., Behrens, T.E., Johansen-Berg, H., 2009. Training induces changes in white-matter architecture. Nat. Neurosci. 12, 1370–1371.
Sin, W.C., Haas, K., Ruthazer, E.S., Cline, H.T., 2002. Dendrite growth increased by visual activity requires NMDA receptor and Rho GTPases. Nature 419, 475–480.
Solecki, D.J., Govek, E.-E., Tomoda, T., Hatten, M.E., 2006. Neuronal polarity in CNS development. Genes Dev. 20, 2639–2647.
Taubert, M., Draganski, B., Anwander, A., Müller, K., Horstmann, A., Villringer, A., Ragert, P., 2010. Dynamic properties of human brain structure: learning-related changes in cortical areas and associated fiber connections. J. Neurosci. 30, 11670–11677.
Testa, F., Maguire, A.M., Rossi, S., Pierce, E.A., Melillo, P., Marshall, K., Banfi, S., Surace, E.M., Sun, J., Acerra, C., 2013. Three-year follow-up after unilateral subretinal delivery of adeno-associated virus in patients with Leber congenital Amaurosis type 2. Ophthalmology 120, 1283–1291.
Timmers, I., Roebroeck, A., Bastiani, M., Jansma, B., Rubio-Gozalbo, E., Zhang, H., 2016. Assessing microstructural substrates of white matter abnormalities: a comparative study using DTI and NODDI. PLoS One 11, e0167884.
Tropea, D., Majewska, A.K., Garcia, R., Sur, M., 2010. Structural dynamics of synapses in vivo correlate with functional changes during experience-dependent plasticity in visual cortex. J. Neurosci. 30, 11086–11095.
Tustison, N.J., Avants, B.B., 2013. Explicit B-spline regularization in diffeomorphic image registration. Front. Neuroinf. 7, 39.
Vaillant, A.R., Zanassi, P., Walsh, G.S., Aumont, A., Alonso, A., Miller, F.D., 2002. Signaling mechanisms underlying reversible, activity-dependent dendrite formation. Neuron 34, 985–998.
Wen, J., Zhang, H., Alexander, D.C., Durrleman, S., Routier, A., Rinaldi, D., Houot, M., Couratier, P., Hannequin, D., Pasquier, F., 2019. Neurite density is reduced in the presymptomatic phase of C9orf72 disease. J. Neurol. Neurosurg. Psychiatr. 90, 387–394.
Winston, G.P., Micallef, C., Symms, M.R., Alexander, D.C., Duncan, J.S., Zhang, H., 2014. Advanced diffusion imaging sequences could aid assessing patients with focal cortical dysplasia and epilepsy. Epilepsy Res. 108, 336–339.
Yeh, F.-C., Verstynen, T.D., Wang, Y., Fernández-Miranda, J.C., Tseng, W.-Y.I., 2013. Deterministic diffusion fiber tracking improved by quantitative anisotropy. PLoS One 8, e80713.
Young, J.M., Vandewouw, M.M., Mossad, S.I., Morgan, B.R., Lee, W., Smith, M.L., Sled, J. G., Taylor, M.J., 2019. White matter microstructural differences identified using multi-shell diffusion imaging in six-year-old children born very preterm. Neuroimage Clin 23, 101855.
Yu, H., Majewska, A.K., Sur, M., 2011. Rapid experience-dependent plasticity of synapse function and structure in ferret visual cortex in vivo. Proc. Natl. Acad. Sci. USA 108, 21235–21240.
Zhang, H., Schneider, T., Wheeler-Kingshott, C.A., Alexander, D.C., 2012. NODDI: practical in vivo neurite orientation dispersion and density imaging of the human brain. Neuroimage 61, 1000–1016.
Zhang, H., Yushkevich, P.A., Alexander, D.C., Gee, J.C., 2006. Deformable registration of diffusion tensor MR images with explicit orientation optimization. Med. Image Anal. 10, 764–785.